

## Buckling analysis of thick isotropic rectangular ssfs plates using polynomial displacement functions

<sup>1</sup>Godwin G., <sup>2</sup>Onodagu D. P., <sup>3</sup>Ezeagu A. C.

<sup>1,2 &3</sup> Department of Civil Engineering, Nnamdi Azikiwe University Awka, Anambra State, Nigeria.

Corresponding Author's E-mail: [godwingah79@gmail.com](mailto:godwingah79@gmail.com).

---

### Abstract

This research study focuses on the buckling analysis of an elastic thick isotropic rectangular plate with three edges simply supported and the third edge free (SSFS). The Ritz energy method was employed using Orthogonal Polynomial Displacement Functions (OPDF) and polynomial shear deformation function, denoted as  $f(z)$ . The general governing Equation of the rectangular thick plate was formulated which was further analysed to deduce the non-dimensional critical buckling load parameters of the plate under uniaxial in-plane compressive load  $N_x$ . The meticulous consideration of the SSFS plate involved satisfying pertinent boundary conditions. The stiffness coefficient values were deduced from the employed Orthogonal Polynomial Displacement Functions. The resultant direct governing equation was solved to yield a concise analytical expression, subsequently utilized to generate non-dimensional critical buckling load parameters for the plates. This process was conducted across varying values of the span-depth ratio ( $a/h$ ) and aspect ratios ( $b/a$ ). To ensure the robustness and accuracy of the findings, the results obtained in this study were meticulously compared with the works of other esteemed researchers. This comparative analysis serves to validate the present results, contributing to the scholarly discourse on the buckling behaviour of isotropic thick rectangular plates.

**Keywords:** Buckling, displacement functions, Rectangular, Ritz energy method, Shear rotation

---

### 1. Introduction

A plate is a flat structural element characterized by a transverse dimension or thickness ( $h$ ) significantly smaller in comparison to its length and width. The study is working on Isotropic plates which have uniform material properties in all directions (Onyechere, 2019). The application of thick plates in engineering has witnessed a gradual upsurge over the years, driven by their appealing attributes including lightweight construction, cost-efficiency, and the ability to withstand substantial loads while being adaptable to specific structural demands (Sayyad, Shinde, and Ghugal, 2016). Plate structures find applications across various engineering disciplines, including Mechanical Engineering and Structural Engineering (Onyeka, 2019). In Structural Engineering, plates serve essential roles in roof and floor slabs, bridge deck slabs and more (Onyeka and Okeke, 2021). To harness the characteristics of thick plates effectively, it is imperative to gain a comprehensive understanding of their structural behaviour and failure conditions to ensure safer and more cost-effective designs (Eze, Onyechere, and Anya, 2018).

Plates are commonly categorized as either thick or thin, a distinction reliant on the plate's thickness (Onyeka and Osegbowa, 2020). Structural stability plays a pivotal role in the design of numerous civil, mechanical, and aeronautical structures because plates are predominantly subjected to transverse and compressive loads acting in the middle plane of the plate. In-plane compressive loading occurs when a plate experiences an axial load applied at the boundary parallel to the mid-plane of the plate and distributed throughout its thickness, see Figure 1.1 (Onyechere, 2019)). The

initiation of instability in plate elements under in-plane loads is referred to as "buckling" (Onyeka, Okafor, and Onah, 2021). The "critical buckling load" represents the maximum load at which an axially loaded plate loses its stability (Sayyad and Ghugal, 2014). If in-plane compressive loads surpass their critical values, it results in substantial deflections and bending stresses that eventually culminate in complete plate failure (Onyeka, Okeke, and Wasiu, 2020). To avert such failures, there is a pressing need for more precise and practical investigations into the stability analysis of plates.

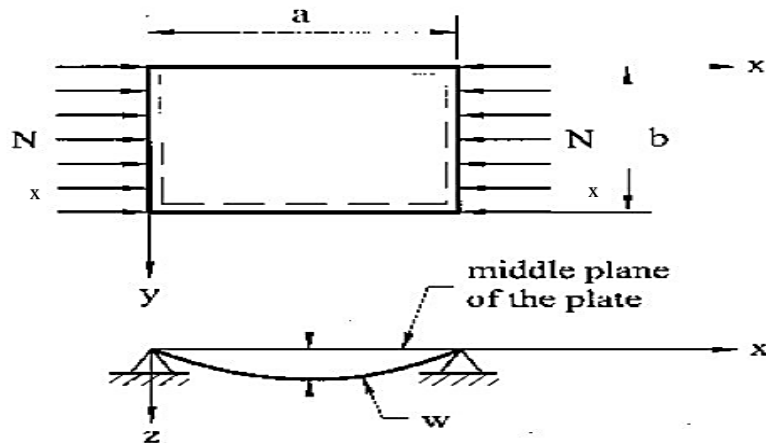


Figure 1.1: Applied Axial compressive forces

The classical plate theory (CPT), introduced by Kirchhoff in 1850, has been found to introduce inaccuracies when the span-to-thickness ratio is relatively low (Onyeka, Mama, and Nwa-David, 2022). While the classical plate theory is suitable for thin plates, it neglects the effects of transverse shear deformation and tends to overestimate the critical buckling loads of thick plates. Therefore, it is recommended to incorporate the effects of shear deformation in cases involving relatively thick plates to ensure reliability (Sayyad, Chikalthankar, and Nandedkar, 2013). In the mid-1900s, the Mindlin first-order shear deformation theory (FSDT) was developed to account for shear deformation effects, permitting transverse shear strains while keeping the shear strains constant across the plate's thickness (Onyeka, 2019). However, both CPT and FSDT fall short of satisfying zero traction boundary conditions on the plate's top and bottom surfaces, necessitating the use of shear correction factors to fulfil constitutive relations for transverse shear stresses and strains (Sayyad and Ghugal, 2014). These limitations led to the development of higher-order shear deformation theories (HSDT) designed to provide a realistic representation of transverse shear strains and stresses across the plate's thickness by assuming parabolic shear strain variations (Nguyen-Thoi, Bui-Xuan, Phung-Van, Nguyen-Xuan, and Ngo-Thanh, 2013).

Recent research has explored various shear deformation theories for the buckling analysis of thick plates, including exponential shear deformation theory, new trigonometric theory, hyperbolic shear deformation theory, and refined trigonometric shear deformation functions (Abdollah, Bahram and Javad, 2016; Eze, Onyechere and Anya, 2018; Gunjal, Hajare Sayyad and Ghodle, 2015; Onyeka and Okeke, 2021; Mahi, Adda-Bedia and Tounsi, 2015; Sayyad and Ghugal, 2014;). Despite these advancements, none of the existing studies have investigated thick plates using polynomial displacement functions within the Ritz energy method. Many researchers resort to thin plate analysis due to the complexity associated with the double Fourier series, highlighting a research gap (Gwarah, 2019). This study aims to address these challenges by investigating the buckling analysis of thick isotropic SSFS rectangular plates using the Ritz energy method with polynomial displacement functions. The utilization of polynomial displacement functions offers a potentially more straightforward and efficient approach to thick plate analysis, contributing to the advancement of knowledge in this field of Engineering.

## 2.0 Material and Methods

### 2.1 Formulation of Direct Governing Equation for Thick Plate Analysis.

The SSFS rectangular thick plate is depicted in Figure 2.1. The plate has a length of ‘a’ in the x-direction, ‘b’ in the y-direction, and a thickness of ‘h’ in the z-direction. It is assumed that the z-direction is positive when facing downward. The plate occupies an area in a Cartesian coordinates system where  $0 \leq x \leq a$ ,  $0 \leq y \leq b$ , and  $-h/2 \leq z \leq$

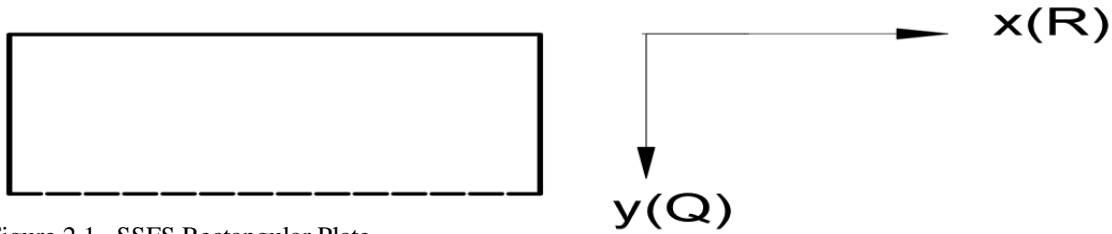


Figure 2.1. SSFS Rectangular Plate

$h/2$ . The aspect ratio is determined by  $b/a$ . Non-dimensional coordinates  $R = x/a$  in the x-direction and  $Q = y/b$  in the y-direction occupying the domain  $0 \leq R \leq 1$  and  $0 \leq Q \leq 1$ . The study of buckling in plates is a crucial aspect of plate analysis, as it helps to identify the critical buckling loads of a plate.

The first step in this section is to utilize the theory of elasticity in plate analysis to identify a variety of plate stresses. These stresses are then condensed into Total Potential Energy functional, which ultimately allows the establishment of the Direct Governing Equation for the thick plate.

**2.1.1 Stress-Displacement Equations.**

The stress displacement equations, as deduced from Equations (2.1a) to (2.1e), emanate from a meticulous analysis of the displacement field, the Strain-Displacement Relation, and the Constitutive (stress-strain) Relations.

$$\sigma_x = \frac{E}{1-\nu^2} \left[ [-j_1 z + j_2 F(z)] \frac{d^2 H}{dx^2} + \nu [-j_1 z + j_3 F(z)] \frac{d^2 H}{dy^2} \right] \tag{2.1a}$$

$$\sigma_y = \frac{E}{1-\nu^2} \left[ \nu z \left( -j_1 + \frac{F(z)}{z} j_2 \right) \frac{d^2 H}{dx^2} + [-j_1 z + j_3 F(z)] \frac{d^2 H}{dy^2} \right] \tag{2.1b}$$

$$\tau_{xy} = \frac{E(1-\nu)}{2(1-\nu^2)} [-2j_1 z + j_2 F(z) + j_3 F(z)] \frac{d^2 H}{dx dy} \tag{2.1c}$$

$$\tau_{xz} = \frac{E(1-\nu)}{2(1-\nu^2)} j_2 \frac{dF(z)}{dz} \frac{dH}{dx} \tag{2.1d}$$

$$\tau_{yz} = \frac{E(1-\nu)}{2(1-\nu^2)} j_3 \frac{dF(z)}{dz} \frac{dH}{dy} \tag{2.1e}$$

Where

$j_i$  are the coefficients of integration or deflection.

$F(z)$  the shear deformation function along the z-direction

**2.1.2 Total potential energy.**

The total potential energy,  $\Pi$ , is mathematically determined in Equation (2.1):

$$\Pi = U + \Omega \tag{2.1f}$$

Where:

$$U = \int_x \int_y \left[ \int_{-\frac{h}{2}}^{\frac{h}{2}} \sigma \cdot \epsilon dz \right] dx dy \tag{2.2a}$$

Expanding Equation (2.2a), Equation (2.2b) is obtained.

$$U = \int_x \int_y \left[ \int_{-\frac{h}{2}}^{\frac{h}{2}} (\sigma_x \epsilon_x + \sigma_y \epsilon_y + \tau_{xy} \gamma_{xy} + \tau_{xz} \gamma_{xz} + \tau_{yz} \gamma_{yz}) dz \right] dx dy \tag{2.2b}$$

Substituting Equations (2.1a) to (2.1e) into Equation (2.2b), Equation (2.2c) is obtained.

$$U = \frac{E}{1-\nu^2} \left[ z^2 j_1^2 - 2j_1 j_2 z F(z) + j_2^2 F(z)^2 \right] \left( \frac{d^2 H}{dx^2} \right)^2 + \frac{E}{1-\nu^2} \left[ z^2 j_1^2 - 2j_1 j_3 z F(z) + j_3^2 F(z)^2 \right] \left( \frac{d^2 H}{dx^2} \right)^2 + \frac{E(1-\nu)}{2(1-\nu^2)} [4j_1^2 z^2 - 4j_1 j_2 z F(z) - 4j_1 j_3 z F(z) + j_2^2 F(z)^2 + 2j_2 j_3 F(z)^2 + j_3^2 F(z)^2] \left( \frac{d^2 H}{dx dy} \right)^2 + j_2^2 \left[ \frac{dF(z)}{dz} \right]^2 \frac{E(1-\nu)}{2(1-\nu^2)} \left( \frac{dH}{dx} \right)^2 + j_3^2 \left[ \frac{dF(z)}{dz} \right]^2 \frac{E(1-\nu)}{(1-\nu^2)} \left( \frac{dH}{dy} \right)^2 \quad (2.2c)$$

$$\Omega = Nx/2 \int_x \int_y (\partial w / \partial x)^2 \partial x \partial y \quad (2.3)$$

Where:

$\Pi$  is the total potential energy of the system.

U the strain energy of deformation (the potential of internal forces).

$\Omega$  the potential energy of external forces (the potential of external forces).

$N_x$  the axial compressive load applied at the mid-plane of the plate.

$\nu$  the poisson's ratio.

Integrating the total potential energy functional within the intervals of the non-dimensional parameters in the  $x$  and  $y$  directions, Equation (2.6) is obtained.

$$\Pi = \frac{abD}{2a^4} \int_0^1 \int_0^1 [q_1 j_1^2 - 2q_1 j_2 + q_3 j_2^2] \left( \frac{d^2 H}{dR^2} \right)^2 + \frac{1}{\beta^2} [2q_1 j_1^2 - 2q_2 j_1 j_2 - 2q_2 j_1 j_3] \left( \frac{d^2 H}{dRdQ} \right)^2 + \frac{(1+\nu)}{\beta^2} g_3 j_2 j_3 \left( \frac{d^2 H}{dRdQ} \right)^2 + \frac{(1-\nu)}{2\beta^2} [q_3 j_2^2 + q_3 j_3^2] \left( \frac{d^2 H}{dQ^2} \right)^2 + \frac{(1-\nu)\rho^2}{2} q_4 j_2^2 \left( \frac{dH}{dR} \right)^2 + \frac{(1-\nu)\rho^2}{2\beta^2} q_4 j_3^2 \left( \frac{dH}{dQ} \right)^2 \Big] dRdQ - \frac{Nx}{2} \int_0^1 \int_0^1 \left( \frac{\partial w}{\partial x} \right)^2 dRdQ \quad (2.4)$$

$$\rho = a/h \quad (2.5)$$

$$\beta = b/a \text{ and } b = a\beta \quad (2.6)$$

$a$  is the length of the plate along the  $x$ -axis.

$b$  is the breadth of the plate along the  $y$ -axis and  $h$  is the thickness of the plate along the  $z$ -axis.

### 2.1.3 Direct governing equation.

To establish the governing equation for the thick plate, the Ritz method is employed, involving the minimization of the potential energy functional by differentiating it with respect to the three coefficients of displacement, namely  $J_1$ ,  $J_2$ , and  $J_3$ . Simultaneously solving the three equations derived from this process yields the direct governing equation for the thick plate.

$$\frac{d\Pi}{dJ_1} = \frac{d\Pi}{dJ_2} = \frac{d\Pi}{dJ_3} = 0 \quad (2.7)$$

Substituting Equation (2.4) into Equation (2.7), Equations (2.8) to (2.10a) are obtained.

$$\frac{d\Pi}{dJ_1} = \frac{D}{a^4} \int_0^1 \int_0^1 [J_1 + q_2 j_2] \left( \frac{d^2 H}{dR^2} \right)^2 + \frac{1}{\beta^2} [2q_1 j_1 + q_2 j_2 + q_3 j_3] \left( \frac{d^2 H}{dRdQ} \right)^2 \Big] dx dy^2 - \int_0^1 \int_0^1 \frac{dFF}{dc_1} dRdQ = 0 \quad (2.8)$$

$$\begin{aligned} \frac{d\Pi}{dj_2} &= \frac{D}{a^4} \int_0^1 \int_0^1 [q_3j_2 - q_2j_1] \left(\frac{d^2H}{dR^2}\right)^2 + \frac{1}{\beta^2} [-q_2j_1] \left(\frac{d^2H}{dRdQ}\right)^2 \\ &+ \frac{(1-v)}{\beta^2} \left[\frac{1}{2}q_3j_3\right] \left(\frac{d^2H}{dRdQ}\right)^2 + \frac{(1-v)}{2\beta^2} [q_3j_2] \left(\frac{d^2H}{dQ^2}\right)^2 + \frac{(1-v)}{2} (q_4j_2) \left(\frac{dH}{dR}\right)^2 \Big] dRdQ = 0 \end{aligned} \tag{2.9}$$

$$\begin{aligned} \frac{d\Pi}{dj_3} &= \frac{D}{a^4} \int_0^1 \int_0^1 \frac{1}{\beta^2} [-q_2j_1] \left(\frac{d^2H}{dRdQ}\right)^2 + \frac{(1-v)}{\beta^2} \left[\frac{1}{2}q_3j_2\right] \left(\frac{d^2H}{dRdQ}\right)^2 \\ &+ \frac{(1-v)}{2\beta^2} [q_3j_3] \left(\frac{d^2H}{dQ^2}\right)^2 + \frac{(1-v)\rho^2}{2\beta^2} (q_4j_3) \left(\frac{dH}{dQ}\right)^2 \Big] dRdQ = 0 \\ & - \frac{abNxj_1^2}{2} \int_0^1 \int_0^1 \left(\frac{\partial w}{\partial x}\right)^2 dRdQ \end{aligned} \tag{2.10a}$$

A parameter  $\lambda_{ij}$  is introduced in Equation (2.10b). Deducing their values from Equations (2.8) to (2.10a), Equation (2.10b) is obtained.

$$\begin{aligned} \lambda_{11} &= q_1 \left(k_1 + 2\frac{k_2}{\beta^2} + \frac{k_3}{\beta^4}\right), \lambda_{12} = -q_2 \left(k_1 + \frac{k_2}{\beta^2}\right), \lambda_{13} = -q_2 \left(\frac{k_2}{\beta^2} + \frac{k_3}{\beta^4}\right) \\ \lambda_{22} &= q_3k_1 + \frac{(1-v)}{2\beta^2} q_3k_2 + \frac{(1-v)\rho^2}{2} q_4k_4, \\ \lambda_{23} &= \frac{(1+v)}{2\beta^2} q_3k_2, \lambda_{33} = \frac{(1-v)}{2\beta^2} q_3k_2 + \frac{1}{\beta^4} q_3k_3 + \frac{(1-v)\rho^2}{2\beta^2} q_4k_5 \end{aligned} \tag{2.10b}$$

The stiffness coefficient  $k_i$  expressions were also deduced from Equation (2.8) to (2.10a). They are obtained here as Equation (2.10c).

$$\begin{aligned} k_1 &= \int_0^1 \int_0^1 \left(\frac{d^2H}{dR^2}\right)^2 dRdQ, k_2 = \int_0^1 \int_0^1 \left(\frac{d^2H}{dRdQ}\right)^2 dRdQ, k_3 = \int_0^1 \int_0^1 \left(\frac{d^2H}{dQ^2}\right)^2 dRdQ \\ k_4 &= \int_0^1 \int_0^1 \left(\frac{dH}{dR}\right)^2 dRdQ, k_5 = \int_0^1 \int_0^1 \left(\frac{dH}{dQ}\right)^2 dRdQ, k_6 = -\frac{ab}{2} \int_0^1 \int_0^1 \frac{Nxj_1^2}{a^2} dRdQ \end{aligned} \tag{2.10c}$$

Defining the  $q_i$  values in Equations (2.8) to (2.10a), Equation (2.10d) is obtained.

$$\begin{aligned} \bar{A} &= \frac{h^3}{12}, q_1 = \frac{\left(\int_{-\frac{h}{2}}^{\frac{h}{2}} z^2 dz\right)}{\bar{A}} = 1, q_2 = \frac{\left(\int_{-\frac{h}{2}}^{\frac{h}{2}} zF(z) dz\right)}{\bar{A}}, q_3 = \frac{\left(\int_{-\frac{h}{2}}^{\frac{h}{2}} F(z)^2 dz\right)}{\bar{A}}, \\ \rho^2 q_4 &= \frac{\left(\int_{-\frac{h}{2}}^{\frac{h}{2}} \left[\frac{dF(z)}{dz}\right]^2 dz\right)}{\bar{A}} \end{aligned} \tag{2.10d}$$

Deducing Equation (2.10b) to matrix form, Equation (2.11) is obtained.

$$\begin{bmatrix} \lambda_{11} & \lambda_{12} & \lambda_{13} \\ \lambda_{21} & \lambda_{22} & \lambda_{23} \\ \lambda_{31} & \lambda_{32} & \lambda_{33} \end{bmatrix} \begin{bmatrix} j_1 \\ j_2 \\ j_3 \end{bmatrix} = \frac{\alpha^4}{D} \begin{bmatrix} \frac{Nx}{a^2} k_4 j_1 \\ 0 \\ 0 \end{bmatrix} \tag{2.11}$$

$$\text{Let } \Gamma_{ij} = \lambda_{ij} \times \frac{1}{k_4} \tag{2.12}$$

Equation (2.12) is the direct governing Equation for thick rectangular plates (using traditional third-order shear deformation theory) of arbitrary boundary conditions.

Dividing through Equation (2.11) by Equation (2.12), Equation (2.13) is obtained

$$\begin{bmatrix} \Gamma_{11} & \Gamma_{12} & \Gamma_{13} \\ \Gamma_{21} & \Gamma_{22} & \Gamma_{23} \\ \Gamma_{31} & \Gamma_{32} & \Gamma_{33} \end{bmatrix} \begin{bmatrix} j_1 \\ j_2 \\ j_3 \end{bmatrix} = \frac{a^2 N_{xcr}}{D} \begin{bmatrix} j \\ 0 \\ 0 \end{bmatrix} \quad (2.13)$$

Determining the determinant of the matrix in Equation (2.13), Equation (2.14) is obtained.

$$\Gamma_{11} + \Gamma_{12} \left[ \frac{-\Gamma_{23}\Gamma_{31} + \Gamma_{33}\Gamma_{21}}{\Gamma_{23}\Gamma_{32} - \Gamma_{33}\Gamma_{22}} \right] + \Gamma_{13} \left[ \frac{-\Gamma_{23}\Gamma_{21} + \Gamma_{22}\Gamma_{31}}{\Gamma_{32}\Gamma_{23} - \Gamma_{33}\Gamma_{22}} \right] = \frac{a^2 N_{xcr}}{D} \quad (2.14)$$

For nontrivial solutions to be viable, the determinant of the coefficient matrix in Equation (2.14) must equate to zero. This condition establishes expression (2.15) as the non-dimensional critical buckling load parameter for the thick plate.

$$\Gamma_{11} + \Gamma_{12} \left[ \frac{-\Gamma_{23}\Gamma_{31} + \Gamma_{33}\Gamma_{21}}{\Gamma_{23}\Gamma_{32} - \Gamma_{33}\Gamma_{22}} \right] + \Gamma_{13} \left[ \frac{-\Gamma_{23}\Gamma_{21} + \Gamma_{22}\Gamma_{31}}{\Gamma_{32}\Gamma_{23} - \Gamma_{33}\Gamma_{22}} \right] = \frac{a^2 N_{xcr}}{D} = \Phi_a \quad (2.15)$$

Substituting  $\rho = a/h$  and the D value into the right side of Equation (2.14) and making  $N_{xcr}$  the subject of the formula, Equation (2.16) is obtained.

$$N_{xcr} = \phi_a * \frac{Eh}{12(1-\nu^2)} * \frac{h^2}{a^2} \quad (2.16)$$

$$D = \frac{Eh^3}{12(1-\nu)} \quad (2.17)$$

$$\frac{b^2 N_{xcr}}{D\beta^2} = \Phi_a \quad (2.18)$$

$$\frac{b^2 N_{xcr}}{D} = \beta^2 \Phi_a = \Phi_b \quad (2.19)$$

With Further simplifications, Equations (2.20) and (2.21) are obtained

$$\psi_a = \phi_a * \left( \frac{1}{\rho^2} \right) = \frac{\phi_a}{\rho^2} \quad (2.20)$$

$$\psi_b = \phi_b * \left( \frac{1}{\rho^2} \right) = \frac{\phi_b}{\rho^2} = \frac{\phi_a \beta^2}{\rho^2} \quad (2.21)$$

Where:

D is the flexural rigidity of the plate.

$N_{xcr}$  is the critical buckling in-plane load applied to the plates under study.

$\phi_a$  is the non-dimensional critical buckling load parameter of the plate in the x-direction and.

$\phi_b$  the non-dimensional critical buckling load parameter of the plate in the y-direction.

## 2.2 Formulation of Polynomial Shear Deformation Function.

The polynomial shear deformation function  $f(z)$  delineates the deformed configuration of the normal to the mid-plane of the plate during deformation. This function, derived through the Touratier model in 1991, is formulated herein as Equation (2.22).

$$f(z) = \frac{z}{5} \left[ \frac{99}{20} - 7 \left( \frac{z}{h} \right)^2 \right] \quad (2.22)$$

$$S = \frac{z}{h} \text{ or } z = hz \quad (2.23)$$

Where:

‘S’ is a non-dimensional parameter along the z-axis, and ‘h’ is the thickness of the plate

With the shear deformation function  $f(z)$  established, the  $q_i$  values in Equation (2.10d) will be obtained as in Equations (2.23a) to (2.23d).

$$q_1 = \frac{\left(\int_{-\frac{h}{2}}^{\frac{h}{2}} z^2 dz\right)}{\bar{A}} = 1 \tag{2.23a}$$

$$q_2 = \frac{\left(\int_{-\frac{h}{2}}^{\frac{h}{2}} zF(z) dz\right)}{\bar{A}}, \quad \int_{-\frac{h}{2}}^{\frac{h}{2}} zF(z) dz = \left[\frac{99z^3}{300} - \frac{7}{25} \left(\frac{z}{h}\right)^5\right]_{-\frac{h}{2}}^{\frac{h}{2}} = \left[\frac{99h^3}{2400} - \frac{7h^5}{800h^2}\right] * 2 =$$

$$q_2 = \frac{13h^3}{200} * \frac{12}{h^3} = 0.78 \tag{2.23b}$$

$$q_3 = \frac{\left(\int_{-\frac{h}{2}}^{\frac{h}{2}} F(z)^2 dz\right)}{\bar{A}}, \quad \int_{-\frac{h}{2}}^{\frac{h}{2}} (F(z))^2 dz = \left[\frac{980z^3}{30000} - \frac{695z^5}{1250h^2} + \frac{49z^7}{175h^4}\right]_{-\frac{h}{2}}^{\frac{h}{2}} =$$

$$q_3 = \frac{2052h^3}{40000} * \frac{12}{t^3} = 0.6156 \tag{2.23c}$$

$$\frac{\rho^2}{a^2} q_4 = \frac{\left(\int_{-\frac{h}{2}}^{\frac{h}{2}} \left[\frac{dF(z)}{dz}\right]^2 dz\right)}{\bar{A}}, \quad \left(\int_{-\frac{h}{2}}^{\frac{h}{2}} \left[\frac{dF(z)}{dz}\right]^2 dz\right) = \left[\frac{9801z}{10000} - \frac{2079z^3}{750} + \frac{441z^5}{125h^4}\right]_{-\frac{h}{2}}^{\frac{h}{2}} =$$

$$q_4 = 6.0912 \tag{2.23d}$$

Summarizing  $q_i$  values, Equation (2.23e) is obtained.

$$q_1 = 1, \quad q_2 = 0.78, \quad q_3 = 0.6156, \quad q_4 = 6.0912 \tag{2.23e}$$

**2.3 Rectangular Thick Plate with three Edges Simply Supported and the third edge free (SSFS)**

The overarching polynomial displacement function  $w=(x,y)$ , as formulated by Onyechere (2019), is employed in this study and is expressed through Equations (2.24) and (2.25).

$$w_x = a_0 + a_1R + a_2R^2 + a_3R^3 + a_4R^4 + a_5R^5 \tag{2.24}$$

$$w_y = a_0 + a_1Q + a_2Q^2 + a_3Q^3 + a_4Q^4 + a_5Q^5 \tag{2.25}$$

Where,

$w_x$  is the out-of-plane displacement along the x-axis and

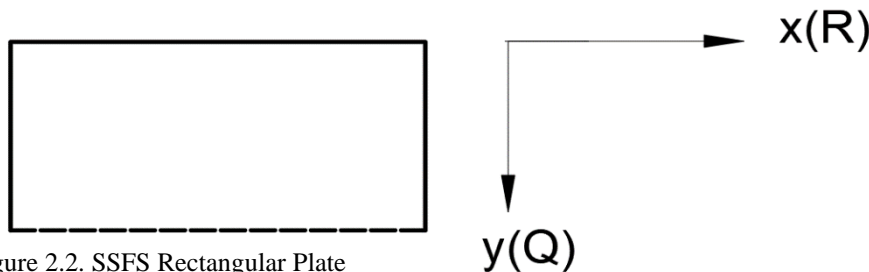


Figure 2.2. SSFS Rectangular Plate

$w_y$  is the out-of-plane displacement along the y-axis

$$w = w_x \cdot w_y = (a_0 + a_1R + a_2R^2 + a_3R^3 + a_4R^4 + a_5R^5)(a_0 + a_1Q + a_2Q^2 + a_3Q^3 + a_4Q^4 + a_5Q^5) \quad (2.26a)$$

The boundary conditions for the SSFS rectangular thick plate as shown in Figure 2.2 are presented in Equations (2.26b) for the R-direction and Equation (2.26c) for the Q-direction. Ibearugbulem et.al (2014) assumed the value of slope to be equal to  $(-2/3)$  of the deflection coefficient for a pin-free strip case (S-F).

R – Direction

$$\begin{aligned} \text{At } R = 0, w_x = 0; \text{ At } R = \frac{1}{2}, \frac{\partial w}{\partial R} = 0; \text{ At } R = 0, \frac{\partial^2 w}{\partial R^2} = 0; \text{ At } R = 1, w_1 = 0; \quad \text{At } R = 1, \frac{\partial^2 w}{\partial w^2} = 0; \\ \text{At } R = \frac{1}{2}, \frac{\partial^3 w}{\partial w^3} = 0; \end{aligned} \quad (2.26b)$$

Q –Direction (Free end at Q=1)

$$\text{At } Q = 0, w_y = 0; \text{ At } Q = 1, \frac{\partial w}{\partial Q} = -\frac{2a_5}{3}; \text{ At } Q = 0, \frac{\partial^2 w}{\partial Q^2} = 0; \text{ At } Q = 1, \frac{\partial^2 w}{\partial Q^2} = 0; \text{ At } Q = 1, \frac{\partial^3 w}{\partial Q^3} = 0 \text{ (Free end) (shear force)} \quad (2.26c)$$

Differentiating Equation (2.24) three times, Equation (2.26d) to (2.26f) are obtained

$$\text{a) } \frac{\partial w}{\partial w} = a_1 + 2a_2R + 3a_3R^2 + 4a_4R^3 + 5a_5R^4 \quad (2.26d)$$

$$\text{b) } \frac{\partial^2 w}{\partial w^2} = 2a_2 + 6a_3R + 12a_4R^2 + 20a_5R^3 \quad (2.26e)$$

$$\text{c) } \frac{\partial^3 w}{\partial w^3} = 6a_3 + 24a_4R + 60a_5R^2 \quad (2.26f)$$

Equation (2.25) should be Differentiated in the same manner as Equation (2.24)

The boundary conditions in Equations (2.26b) in the R-direction and Equation (2.26c) in the Q-direction were substituted into Equations (2.26d) to (2.26f) and the polynomial displacement function for the SSFS plate was determined and presented here as Equation (2.27)

$$w = (w_x, w_y) = -a_4 b_5 (R - 2R^3 + R^4) \left( \frac{7Q}{3} + \frac{10Q^3}{3} - \frac{10Q^4}{3} + Q^5 \right) \quad (2.27)$$

$$\text{Let, } B = -a_4 \cdot b_5 \quad (2.28)$$

$$\text{And } H = (R - 2R^3 + R^4) \left( \frac{7Q}{3} - \frac{10Q^3}{3} + \frac{10Q^4}{3} - Q^5 \right) \quad (2.29a)$$

Where:

$-a_4 \cdot b_5$  is the Amplitude and

$H$  = the Shape Function for SSFS thick rectangular plate.

Differentiating Equation (2.29a) to correspond to the stiffness expressions in Equation (2.10c), Equations (2.29b) to (2.29g) are obtained.

$$\frac{\partial H}{\partial R} = (1 - 6R^2 + 4R^3) \left( \frac{7Q}{3} - \frac{10Q^3}{3} + \frac{10Q^4}{3} - Q^5 \right) \quad (2.29b)$$

$$\frac{\partial^2 H}{\partial R^2} = (-12R + 12R^2) \left( \frac{7Q}{3} - \frac{10Q^3}{3} + \frac{10Q^4}{3} - Q^5 \right) \quad (2.29c)$$

$$\frac{\partial H}{\partial Q} = (R - 2R^3 + R^4) \left( \frac{7}{3} - \frac{30Q^2}{3} + \frac{40Q^3}{3} - 5Q^4 \right) \tag{2.29d}$$

$$\frac{\partial^2 H}{\partial Q^2} = (R - 2R^3 + R^4) \left( -\frac{60Q}{3} + \frac{120Q^2}{3} - 20Q^3 \right) \tag{2.29e}$$

$$\frac{\partial^2 H}{\partial R \partial Q} = (1 - 6R^2 + 4R^3) * \left( \frac{7}{3} - 10Q^2 + \frac{40Q^3}{3} - 5Q^4 \right) \tag{2.29f}$$

$$\left( \frac{\partial H}{\partial R} \right)^2 = \left[ (1 - 6R^2 + 4R^3) \left( \frac{7Q}{3} - \frac{10Q^3}{3} + \frac{10Q^4}{3} - Q^5 \right) \right]^2 \tag{2.29g}$$

**2.3.1 Determination of the stiffness coefficient values for SSFS thick plate**

The stiffness coefficient  $k_i$  expressions were determined in Equation (2.10c). Equations (2.29b) to (2.29g) were substituted into Equation (2.10c) and integrated to obtain the various values of  $k_i$  as summarized here in Equation (2.30).

$$k_1 = 4.025782, k_2 = 0.601361, k_3 = 0.187453, k_4 = 0.407371, k_5 = 0.104661, \\ k_6 = 0.04127 \tag{2.30}$$

**2.4 Numerical example.**

**An Example Illustrating the Buckling Analysis of SSFS Rectangular Plates.**

Consider a plate that is simply supported at its three edges and free at the third edge (SSFS). Let's assume that the aspect ratio, which is the ratio of the plate's width (b) to its length (a) ( $\beta = b/a$ ) is equal to 1. The span-depth ratio, ( $\rho = a/h$ ) which is the ratio of the plate's length (a) to its thickness (h), is equal to 5. The Poisson's ratio, denoted by  $\nu$ , is equal to 0.3. The  $q_i$  values were determined and presented here as Equation (3.1). The non-dimensional critical load parameters are determined in the following Equations.

$$q_1 = 1, \quad q_2 = 0.78, \quad q_3 = 0.6156, \quad q_4 = 6.0912 \tag{2.31}$$

The stiffness coefficient values ' $k_i$ ' in Equation (2.30) are reproduced here as Equation (2.32)

$$k_1 = 4.025782, k_2 = 0.601361, k_3 = 0.187453, k_4 = 0.407371, k_5 = 0.104661, \\ k_6 = 0.04127 \tag{2.32}$$

The expressions for  $\lambda_{ij}$  obtained in Equation (2.10b) are reproduced here as Equation (2.33).

$$\lambda_{11} = q_1 \left( k_1 + 2 \frac{k_2}{\beta^2} + \frac{k_3}{\beta^4} \right), \lambda_{12} = -q_2 \left( k_1 + \frac{k_2}{\beta^2} \right), \lambda_{13} = -q_2 \left( \frac{k_2}{\beta^2} + \frac{k_3}{\beta^4} \right) \\ \lambda_{22} = q_3 k_1 + \frac{(1-\nu)}{2\beta^2} q_3 k_2 + \frac{(1-\nu)\rho^2}{2} q_4 k_4, \\ \lambda_{23} = \frac{(1+\nu)}{2\beta^2} q_3 k_2, \lambda_{33} = \frac{(1-\nu)}{2\beta^2} q_3 k_2 + \frac{1}{\beta^4} q_3 k_3 + \frac{(1-\nu)\rho^2}{2\beta^2} q_4 k_5 \tag{2.33}$$

Substituting the  $k_i$  and  $q_i$  values in Equation (2.32) and (2.31) respectively into Equation (2.33), the  $\lambda_{ij}$  values in Equation (2.33) are obtained in Equation (2.34).

$$\lambda_{11} = 5.415957, \lambda_{12} = -3.6092, \lambda_{13} = -0.6153, \lambda_{22} = 24.3199, \lambda_{23} = 0.2406 \\ \lambda_{33} = 5.8232 \tag{2.34}$$

The  $\Gamma_{ij}$  expressions in Equation (2.12) are reproduced here as Equation (2.35)

$$\Gamma_{ij} = \lambda_{ij} \times \frac{1}{k_4} \quad (2.35)$$

Equation (2.15) is reproduced here as Equation (2.36)

$$\Gamma_{11} + \Gamma_{12} \left[ \frac{-\Gamma_{23}\Gamma_{31} + \Gamma_{33}\Gamma_{21}}{\Gamma_{23}\Gamma_{32} - \Gamma_{33}\Gamma_{22}} \right] + \Gamma_{13} \left[ \frac{-\Gamma_{23}\Gamma_{21} + \Gamma_{22}\Gamma_{31}}{\Gamma_{32}\Gamma_{23} - \Gamma_{33}\Gamma_{22}} \right] = \frac{a^2 N_{xcr}}{D} = \Phi_a \quad (2.36)$$

The  $\Gamma_{ij}$  values are determined by substituting Equation (3.3a) into Equation (3.2b).

The  $\Gamma_{ij}$  values obtained from Equation (2.34) are substituted into Equation (2.36). The non-dimensional critical buckling load parameters for the SSFS thick plate in the x and y directions are obtained in Equations (2.37) and (2.38).

$$\frac{a^2 N_{xcr}}{D} = \phi_a = 11.8384 \quad (2.37)$$

$$\Phi_b = \frac{b^2 N_{xcr}}{D} = \beta^2 \phi_a = 11.8384 * 1^2 = 11.8384 \quad (2.38)$$

Substituting Equation (2.38) into Equation (2.21), Equation (2.39) is obtained.

$$\psi_b = 11.8384 * \frac{1^2}{5^2} = 0.4735 \quad (2.39)$$

### 3.0 Results and Discussions

#### 3.1. Results Presentation

The non-dimensional critical buckling load parameter  $\phi_a$  and  $\Phi_b$  of thick rectangular SSFS plate for span depth ratio ( $\rho = a/h = 5$ ) and aspect ratio ( $\beta = b/a = 1$ ) were obtained in Equations (2.37) and (2.38) and summarised here as Equation 3.1)

$$\phi_a = 11.8384, \quad \Phi_b = 11.8384, \quad (3.1)$$

The objective of this numerical illustration is to exemplify the computation of non-dimensional critical load parameters across varying aspect and span-depth ratios. The selection of the SSFS plate for this example is deliberate, as other configurations such as SSSS plate have been extensively examined in existing literature.

##### 3.1.1. Buckling analysis of SSFS thick plates.

Table 3.1 provides a comparative analysis between the current investigation and previous research conducted by Onyechere (2019) and Ezeh et al. (2018). Additionally, the table presents non-dimensional critical buckling load parameters for the SSFS thick plate for this study, encompassing various values of span-depth ratios ( $\rho = a/h$ ) and aspect ratios ( $\beta = b/a$ ).

Table 3.1: Results of the Present Study Compared with the Results of Other Researchers for SSFS thick Plate.

$\phi_a = \frac{a^2 N_{xcr}}{D}$		$\beta = b/a$						
		1.0	1.1	1.2	1.4	1.6	1.8	2
$\rho = a/h$	Theory							
5	Present Study (P.S)	11.8384	11.2923	10.8837	10.3258	9.9728	9.7354	9.5682
	Onyechere (2019), (O)	11.8382	11.2714	10.8552	10.2960	9.9467	9.7134	9.5498
	Ezeh <i>et al.</i> (2018), (E)	11.8382	11.2920	10.8835	10.3256	9.9726	9.7352	9.5680
	% Difference btw P.S and O	0.0017	0.1851	0.2619	0.2886	0.2617	0.2260	0.1923
	% Difference btw P.S and E	0.0017	0.0027	0.0018	0.0019	0.0020	0.0021	0.0021
10	Present Study (P.S)	12.8975	12.2703	11.8086	11.1870	10.7981	10.5383	10.3560
	Onyechere (2019), (O)	12.8974	12.2646	11.8008	11.1869	10.7910	10.5323	10.3509
	Ezeh <i>et al.</i> (2018), (E)	12.8974	12.2702	11.8085	11.1869	10.7980	10.5382	10.3559
	% Difference btw P.S and O	0.0008	0.0465	0.0661	0.0009	0.0658	0.0569	0.0492
	% Difference btw P.S and E	0.0008	0.0008	0.0008	0.0009	0.0009	0.0009	0.0010
20	Present Study (P.S)	13.1932	12.5429	12.0661	11.4263	11.0272	10.7610	10.5743
	Onyechere (2019), (O)	13.1932	12.5756	12.0641	11.4242	11.0254	10.7595	10.5730
	Ezeh <i>et al.</i> (2018), (E)	13.1932	12.5429	12.0660	11.4263	11.0272	10.7610	10.5743
	% Difference btw P.S and O	0.0000	-0.2607	0.0166	0.0184	0.0163	0.0139	0.0123
	% Difference btw P.S and E	0.0000	0.0000	0.0008	0.0000	0.0000	0.0000	0.0000
50	Present Study (P.S)	13.2785	12.6216	12.1403	11.4952	11.0932	10.8251	10.6371
	Onyechere (2019), (O)	13.2785	12.6213	12.1400	11.4949	11.0929	10.8249	10.6369
	Ezeh <i>et al.</i> (2018), (E)	13.2785	12.6215	12.1403	11.4952	11.0932	10.8251	10.6371
	% Difference btw P.S and O	0.0000	0.0024	0.0025	0.0026	0.0027	0.0018	0.0019
	% Difference btw P.S and E	0.0000	0.0008	0.0000	0.0000	0.0000	0.0000	0.0000
100	Present Study (P.S)	13.2908	12.6329	12.1510	11.5051	11.1027	10.8343	10.6462
	Onyechere (2019), (O)	13.2908	12.6328	12.1509	11.5051	11.1026	10.8343	10.6461
	Ezeh <i>et al.</i> (2018), (E)	13.2908	12.6329	12.1510	11.5051	11.1027	10.8343	10.8343
	% Difference btw P.S and O	0.0000	0.0008	0.0008	0.0000	0.0009	0.0000	0.0009
	% Difference btw P.S and E	0.0000	0.0000	0.0000	0.0000	0.0000	0.0000	-1.7668

**3.2. Discussions on the non-dimensional critical Buckling load parameters of the SSFS Thick Isotropic Rectangular Plate.**

In Table 3.1, when considering an aspect ratio ( $\beta$ ) of 1 and a span-depth ratio ( $\rho$ ) of 5, the non-dimensional critical buckling parameter ( $\phi_a$ ) is recorded as 11.8384. Conversely, at an equivalent span-depth ratio ( $\rho$ ) of 5 and an aspect ratio ( $\beta$ ) of 2, the non-dimensional critical buckling parameter ( $\phi_a$ ) is noted as 9.5682. The discernible reduction in the non-dimensional critical buckling load parameters as the aspect ratio increases suggests an elevated susceptibility of the plate to buckling. This observation holds significance for engineers involved in the optimization of plate designs, emphasizing the need to ensure structural stability under diverse loading conditions.

In contrast, at a span-depth ratio ( $\rho$ ) of 5, the non-dimensional critical buckling load parameter is measured at 11.8384. At a subsequent span-depth ratio ( $\rho$ ) of 100, the non-dimensional critical buckling load parameter elevates to 13.2908. This increase implies enhanced stability, as a higher non-dimensional critical buckling load parameter necessitates greater loads to induce instability. Such findings are pertinent to structural engineers seeking to optimize designs for improved stability, particularly in applications where resistance to buckling is paramount.

Table 3.1 presents a comprehensive comparison of the non-dimensional critical buckling load parameter values obtained in this study with those derived from the investigations conducted by Ezeh *et al.* (2018) and Onyechere (2019). The percentage differences between the non-dimensional critical buckling load parameters of this study and the referenced studies are consistently minimal, with a maximum value of 1.7668% observed at an aspect ratio ( $\beta = b/a$ ) of 1 and a span depth ratio ( $\rho = a/h$ ) of 100, corresponding to the research conducted by Ezeh *et al.* (2018). Notably,

the minimum percentage difference recorded is 0.0000%, corresponding to the comparison between Ezeh et al. (2018) and Onyechere (2019) at an aspect ratio ( $\beta = b/a$ ) ranging from 1 to 1.8 and a span depth ratio ( $\rho = a/h$ ) of 100.

It is crucial to emphasize that any result falling within the range of 0% to 5% is considered acceptable in engineering calculations, aligning with established statistical principles for result comparison. Therefore, the findings of this study affirm its reliability and provide a robust solution for the buckling analysis of isotropic thick rectangular plates.

#### 4.0. Conclusion

Based on the findings of this study, it can be concluded that:

The non-dimensional critical buckling load parameter Equation, derived from the simultaneous Equations of the governing equation employed in this study, yields precise and satisfactory results for the buckling analysis of isotropic thick rectangular plates.

The third-order polynomial shear deformation function  $F(z)$ , formulated for this study, demonstrates its effectiveness by producing results that align with acceptable statistical intervals when compared with other research endeavours, as delineated in Table 4.1. This function introduces a parabolic variation of transverse shear strains and stresses across the plate thickness, eliminating the necessity for a shear correction factor employed in the first-order shear deformation theory (FSDT).

The general Orthogonal Polynomial Displacement Functions 'w,' employed for the analysis of isotropic rectangular thick SSFS plates, exhibit notable adaptability for plates featuring various boundary conditions, requiring no intricate mathematical formulations.

The stiffness coefficient values ( $k_i$ ) determined for the rectangular thick plate with SSFS boundary conditions in this research exhibit high reliability and consistency with the findings of Ezeh et al. (2018) and Onyechere (2019).

#### 5.0 Recommendation

- i) This research employs the user-friendly Shear Deformation Function  $F(z)$  for thick plate analysis. Designers are encouraged to utilize this function, as its results are both reliable and efficient.
- ii) The Orthogonal Polynomial Displacement Functions developed for this study prove highly effective for analyzing thick rectangular SSFS plates. It is suggested that this efficiency could extend to other complex plate systems with multiple unsupported edges.
- iii) Future researchers should consider applying the theories presented in this study to explore the combined effects of in-plane compression, transverse, and dynamic loads on thick rectangular plates.
- iv) To achieve more efficient results for critical buckling load of thick plates, it is recommended that further research be conducted on the Shear Deformation Theory using the fifth and seventh order.

#### 5.2. Contribution to Knowledge:

This study introduces a novel simultaneous linear equation, defined as the direct governing Equation of the plate, establishing a clear relationship between the plate's stiffness and the applied buckling load see Equations (2.10b) and (2.11). Unlike prevalent equations in the literature, often characterized by parabolic complexity, the proposed linear equation offers a straightforward and less cumbersome approach for efficient solutions.

In contrast to existing equations prevalent in thick plate analysis, which frequently adopt parabolic forms posing challenges in terms of computational complexity, the linear equation proposed in this study enhances solvability. Its straightforward nature facilitates ease of computation, providing a more accessible method for researchers and practitioners in the field of Engineering.

In essence, these contributions enhance the overall understanding and practical utility of thick plate analysis, providing a more accessible framework for researchers and engineers engaged in structural analysis and design.

## References

- Abdollah, M., Bahram, N. N., and Javad, V. A. 2016. 3-D elasticity buckling solution for simply supported thick rectangular plates using displacement potential functions. *Applied Mathematical Modelling*, 40, 5717-5730.
- Eze, J. C., Onyechere, i. c., and Anya, u. c. 2018. Buckling analysis of thick isotropic plates by using exponential shear deformation theory. *International Journal of Scientific and Engineering Research*, 9(9).
- Gunjal, S. M., Hajare, R. B., Sayyad, A. S., and Ghodle, M. D. 2015. Buckling Analysis of Thick Plates using Refined Trigonometric Shear Deformation Theory. *Journal of Materials and Engineering Structures*, 2, 159-167.
- Gwarah, L. S. (2019). Application of Shear Deformation Theory in the Analysis of Thick Rectangular Plate Using Polynomial Displacement Function. *A Thesis Presented To The School Of Postgraduate Studies, Federal University Of Technology Owerri* (p. 4).
- Ibearugbulem, O. M., Ezeh, J. C., Nwadike, A. N., and Maduh,, U. J. 2014. Buckling Analysis of Isotropic SSFS Rectangular Plate using Polynomials Shape Function. *International Journal of Emerging Technology and Advanced Engineering*, 4(1), 6
- Mahi, A., Adda-Bedia, E. A., and Tounsi, A. 2015. A new hyperbolic shear deformation theory for bending and free vibration analysis of isotropic functionally graded, sandwich and laminated composite plates. *Applied Mathematical Modelling, Simulation and Computation for Engineering and Environmental Systems*, 39(9), 2489-2508.
- Nguyen-Thoi, T., Bui-Xuan, T., . Phung-Van, P., Nguyen-Xuan, H., and Ngo-Thanh, P. 2013. Static free-vibration and buckling analyses of stiffened plates using triangular elements. *Journal of Computers and Structures*, 125, 100-111.
- Onyechere, I. C. 2019. Stability and Vibration Analysis of Thick Rectangular Plates using Orthogonal Polynomial Displacement Function. *A Thesis Presented To The School Of Postgraduate Studies, Federal University Of Technology Owerri* (p. 10).
- Onyeka,, F. C. 2019. Direct analysis of critical lateral load in a thick rectangular plate using refined plate theory. *International Journal of Civil Engineering and Technology*, 10(5), 492-505.
- Onyeka, F. C., and Okeke, E. T. 2021. Analytical solution of a thick rectangular plate with clamped and free support boundary condition using polynomial shear deformation theory. *Advances in Science, Technology and Engineering Systems Journal*, 6(1), 1427-1439.
- Onyeka, F. C., Okafor, F. O., and Onah, , H. N. 2021. Application of a new trigonometric theory in the buckling analysis of a three-dimensional thick plate. *International Journal of Emerging Technologies*, 12(1), 228-240.
- Onyeka, F. C., Okeke, T. E., and Wasu, J. 2020. Strain-displacement expressions and their effect on the deflection and strength of the plate. *Advances in Science, Technology and Engineering Systems Journal*, 5(5), 401-413.
- Onyeka, F. C., Mama, B. O., and Nwa-David, D. C. 2022. Application of variation method in three-dimensional stability analysis of rectangular plate using various exact shape functions. *Nigerian Journal of Technology*, 41(1), 8-20.
- Onyeka, F. C., and Osegbowa,, D. 2020. Stress analysis of thick rectangular plate using higher order polynomial shear deformation theory. *Futo Journal Series – Futojnls*, 6(2), 142-161.
- Sayyad, I. I., Chikalthankar, S. B., and Nandedkar, V. M. 2013. Trigonometrical shear deformation theory for thick plate analysis. Organized By: SNJB's Late Sau. K. B. Jain College of Engineering, Chandwad.
- Sayyad , A. S., and Ghugal, Y. M. 2014. Buckling and free vibration analysis of orthotropic plates by using exponential shear deformation theory. *Latin American Journal of Solids and Structures*, 11(8).
- Sayyad, A. S., Shinde, B. M., and Ghugal, Y. M. 2016. Bending, vibration and buckling of laminated composite plates using a simple four-variable plate theory. *Latin American Journal of Solids and Structures*, 13(3).